Supplement: Quantum Logic Enhanced Sensing in Solid State Spin Ensembles

Nithya Arunkumar,[1,2,3] Kevin S. Olsson,[3,4,5] Jner Tzern Oon,[3,6] Connor A. Hart,[3,4] Dominik B. Bucher,[1,7] David Glenn,[1] Mikhail D. Lukin,[1] Hongkun Park,[1,8] Donhee Ham,[2] and Ronald L. Walsworth[1,3,4,6]

[1]*Department of Physics, Harvard University, Cambridge, Massachusetts 02138, USA*
[2]*John A. Paulson School of Engineering and Applied Sciences, Harvard University, Cambridge, Massachusetts 02138, USA*
[3]*Quantum Technology Center, University of Maryland, College Park, Maryland 20742, USA*
[4]*Department of Electrical and Computer Engineering, University of Maryland, College Park, Maryland 20742, USA*
[5]*Intelligence Community Postdoctoral Research Fellowship Program, University of Maryland, College Park, Maryland 20742, USA*
[6]*Department of Physics, University of Maryland, College Park, Maryland 20742, USA*
[7]*Department of Chemistry, Technical University of Munich, Germany*
[8]*Department of Chemistry and Chemical Biology, Harvard University, Cambridge, Massachusetts 02138, USA*

(Dated: August 16, 2023)

CONTENTS

I. Experimental Methods 1

II. Signal-to-Noise Ratio with Quantum Logic Enhanced Readout 2

III. AC Magnetometry 3

IV. Considerations for Implementing Quantum Logic Readout in NV Ensembles 4

V. ^{15}N Nuclear spin T1 5

References 6

I. EXPERIMENTAL METHODS

The ensemble NV sensor is a $(2 \times 2 \times 0.5)\,\mathrm{mm}^3$ high purity diamond chip with 13 µm thick, nitrogen-doped layer ($[\mathrm{N}] \approx 14\,\mathrm{ppm}$) grown using a high-purity, chemical vapour deposition process (Element Six, Ltd). After irradiation and annealing, the nitrogen-doped layer contains $[\mathrm{NV}] \approx 2.3\,\mathrm{ppm}$. The NV ensemble dephasing time T_2^*, measured using Ramsey spectroscopy, is $T_2^* \approx 600\,\mathrm{ns}$. The NV ensemble coherence time, measured using a Hahn-echo sequence, is $T_2 \approx 14.5$ µs. The top face of the diamond is cut perpendicular to the [100] crystal axis and the lateral faces are perpendicular to [110]. All four edges of the top face were then polished at 45 degrees (Delaware Diamond Knives), with a top face area of 1 mm × 1 mm, to aid optical illumination of the NV ensemble by 532nm laser light using total internal reflection. The [111] axis of the NV sensor is aligned parallel to a variable bias magnetic field (0 G to 3700 G), generated by a feedback-stabilized electromagnet. Details about the magnetic bias field stabilization is described in the Methods section of Ref. [1].

The 130 mW optical beam ($\lambda = 532\,\mathrm{nm}$), generated by a solid-state laser (Coherent Verdi G7), is focused down to a spot size of about 15 µm on the NV layer and pulsed using an acousto-optic modulator (Gooch & Housego, 3250-220). For the experiments in this work, the duration of optical pulses for NV electronic spin polarization and readout is 2.7 µs. Specifically, the NV spin-state-dependent fluorescence is read out during the first 1 µs of an applied 2.7 µs optical pulse, followed by additional optical re-initialization of the NV electronic spin for 1.7 µs. As described in section V below, optical pulses of variable duration T_{op} were also applied for determination of the ^{15}N nuclear spin lifetime (T_1). The NV fluorescence signal is collected by a liquid light guide (Thorlabs LLG5-8H) and delivered to a photodetector (Thorlabs PDB210A).

An arbitrary waveform generator (Tektronix AWG7122C) generates microwave (MW) pulses with a temporal resolution of 12 Giga-samples per second (83 ps). The pulses are amplified using a microwave amplifier (Minicircuits ZHL-25W-63+, RF Lambda RFLUPA0618GD). The radiofrequency (RF) pulses used to apply the CNOT gate to the NV nuclear spin, conditioned on the NV electronic spin state, are generated by a function generator (Rigol DG1032). This gate, $\mathrm{CNOT}_{n|e}$, is calibrated using the pulse sequence shown in main text Fig. 2(c) with $\mathrm{T_{op}} = 0$, where the

duration of the RF pulse is varied while the spin-state-dependent NV fluorescence contrast is monitored. The RF duration that maximizes the population transfer (i.e., minimizes contrast) in the SWAP operation is used for the $\mathrm{CNOT}_{n|e}$ gate, see main Fig. 2(b). The RF pulses range in frequency from ∼1-3 MHz, depending on the magnetic field strength.

The eigenstates of the composite NV electronic-nuclear system are $|\{\uparrow_e,\downarrow_e\};\{\uparrow_n,\downarrow_n\}\rangle$, where $|\downarrow_e\rangle$ and $|\uparrow_e\rangle$ correspond to electronic states $m_s=0,-1$, and $|\downarrow_n\rangle$ and $|\uparrow_n\rangle$ correspond to the nuclear states $m_I=-\frac{1}{2},\frac{1}{2}$. The $\mathrm{CNOT}_{e|n}$ gate is achieved by applying a selective MW pulse of duration τ and frequency f_1 in order to drive transitions only between the electronic spin states, e.g., $|\downarrow_e;\downarrow_n\rangle \rightarrow |\uparrow_e;\downarrow_n\rangle$. The transitions for the electronic states with $|\uparrow_n\rangle$ are off resonance from the selective pulse, with $f_2=f_1+A$, where $A=3.03$ MHz is the longitudinal component of the hyperfine tensor for ^{15}N. Applying the MW pulse for a Rabi frequency of Ω_1 for the on-resonance transitions leads to a Rabi frequency of $\Omega_2=\sqrt{\Omega_1^2+(2\pi A)^2}$ for the off-resonance transitions. Now, to be spin-state selective, the duration of the MW pulse needs to induce a phase accumulation of $\Omega_1\tau=\pi$ for the on-resonance transition, and $\Omega_2\tau=2\pi$ (i.e., zero phase) for the off-resonance transition. This condition is satisfied with $\tau=\sqrt{3}\,/\,2A$, which is 286 ns for $A=3.03$ MHz, corresponding to $\Omega_1=(2\pi)$ 1.75 MHz and $\Omega_2=(2\pi)$ 3.5 MHz. With this duration τ for the $\mathrm{CNOT}_{e|n}$ gate, the quantum logic readout duration (T_{QLR}) ≈ 3 µs, i.e., $T_{\mathrm{QLR}}\approx T_{\mathrm{CNOT}_{e|n}}+T_{\mathrm{op}}=0.286$ µs + 2.7 µs, with a buffer ∼ 10 ns between the two pulses (see Fig. 3 in the main text).

Both the MW and the RF control pulses are combined using a power splitter (Minicircuits ZN2PD2-14W-S+). The combined signal is delivered to the diamond sensor to drive the NV electronic spins and the ^{15}N nuclear spins, through a shorted, single-loop coil of 1 mm diameter situated about 0.5 mm above the NV ensemble. A synthetic AC magnetic test signal (∼ 1 MHz) is generated by applying an AC voltage (Rigol DG1022) to a home-built multi-loop test coil (4 loops, 10 mm diameter) situated a few mm above the NV -diamond sensor.

II. SIGNAL-TO-NOISE RATIO WITH QUANTUM LOGIC ENHANCED READOUT

In comparing N conventional readouts, the amplitude of each readout A_n corresponds to a measurement of the same spin population. Thus, the signal-to-noise ratio (SNR) for the mean signal of N measurements is simply the average signal divided by the root mean squared error

$$\mathrm{SNR}(N)_{\mathrm{conv.}}=\frac{\sum_{n=1}^{N}A_n}{\sqrt{\sum_{n=1}^{N}\sigma_n^2}}$$

where σ_n is the error (uncertainty) of the n-th measurement. Now with the quantum logic enhanced (QLE) readout, A_n is affected by the decaying spin population of the memory spins, due to their finite lifetime. It is assumed that σ_n remains approximately equivalent to that for conventional readout, as NV ensemble fluorescence measurements are typically not at the photon-shot-noise limit. The effect of decaying A_n can be accounted for by weighting the amplitudes and uncertainties of each measurement when calculating the SNR

$$\mathrm{SNR}(N)_{\mathrm{QLE}}=\frac{\sum_{n=1}^{N}w_nA_n}{\sqrt{\sum_{n=1}^{N}w_n^2\sigma_n^2}}$$

where w_n is the weight of the nth readout. Rewriting the numerator and invoking the Cauchy-Schwarz inequality yields

$$\left(\sum w_n\sigma_n\frac{A_n}{\sigma_n}\right)^2\leq\left(\sum w_n^2\sigma_n^2\right)\left(\sum\frac{A_n^2}{\sigma_n^2}\right).$$

The equality is fulfilled by when $w_n=A_n/\sigma_n^2$, leading the optimal SNR to be [2]

$$\text{Optimal }\mathrm{SNR}(N)_{\mathrm{QLE}}=\sqrt{\sum_{n=1}^{N}\frac{A_n^2}{\sigma_n^2}}.$$

The weighting factor A_n/σ_n^2 agrees with the intuition that measurements with lower signal amplitude should be weighted less when calculating $\mathrm{SNR}(N)_{\mathrm{QLE}}$ than those with higher signal amplitudes.

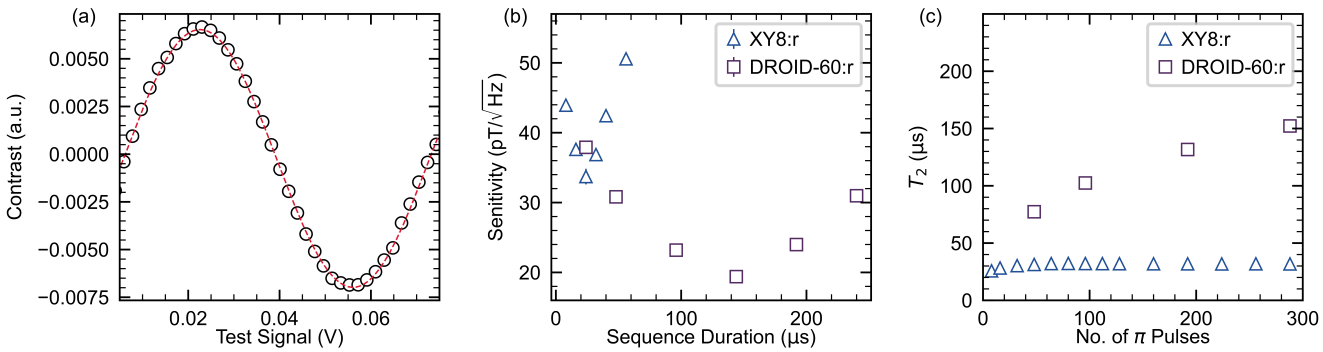


FIG. S1. **AC magnetometry with XY8 and DROID-60. (a)** Measured magnitude of AC magnetic field test signal used in calibration of NV ensemble magnetic field sensitivity using DROID-60:6 and conventional readout. Analogous calibration was performed for each DROID-60:r and XY8:r sequence. **(b)** Measured AC sensitivities, using conventional readout, for XY8:r and DROID-60:r decoupling sequences as a function of sequence duration (proportional to the number of sequence repetitions r). **(c)** Measured NV T_2 for XY8 and DROID-60 dynamical decoupling as a function of the number M of applied π-pulses. The XY8 T_2 saturation is attributed to like-spin, NV-NV interactions.

III. AC MAGNETOMETRY

We characterize the optimal duration for XY8 and DROID-60 sequences by measuring their AC sensitivities using conventional readout – i.e., without the quantum logic enhanced (QLE) protocol – for various sequence durations. The AC magnetic test signal is first calibrated by measuring the signal amplitude (i.e., the NV ensemble fluorescence contrast) as a function of voltage applied to the test coil. The NV contrast undergoes periodic oscillations with increasing test signal voltage (Fig. S1(a) black circles). A single oscillation corresponds to 2π phase accumulation by the NV electronic spins during the sensing sequence. The magnetic signal amplitude that produces 2π phase accumulation is given by

$$\mathrm{B}_{AC}(2\pi) = 2 * \frac{\hbar\pi^2 f_0}{g\mu_B M}, \tag{1}$$

where $g = 2$ is the Landé g-factor, μ_B is the Bohr magneton, f_0 is the frequency of the sensing sequence ($1/2\tau$), and M is the total number of π pulses applied during the r sequence repetitions (or effective π pulses for DROID-60 as it contains pairs of consecutive $\pi/2$ pulses which act as π pulses, for a total of 48 effective π pulses in a single sequence [3, 4]). For DROID-60:6 at $f_0 = 1$ MHz, $\mathrm{B}_{AC}(2\pi) = 0.39(1)$ μT. From the sinusoidal fit to the data (Fig. S1(a) red line), the 2π phase accumulation occurs at 0.0670(4) V. From these two values, we get the calibration constant $\mathrm{B}_{AC}(2\pi)$ / V = 5.81(4) μT/V. A similar process for XY8:6 yields $\mathrm{B}_{AC}(2\pi)$ / V = 11.68(6) μT/V.

The AC sensitivity η is determined by,

$$\eta = \frac{\sigma^{1s}}{|dS/d\mathrm{B}_{AC}|} \tag{2}$$

where σ^{1s} is the uncertainty of the measured NV ensemble fluorescence contrast for 1 second averaging and $|dS/d\mathrm{B}_{AC}|$ is the gradient of the contrast with respect to B_{AC}. Both these parameters are determined at the zero-crossing of the fit to the calibration data, as shown in Fig. S1(a). σ^{1s} is given by the standard error at the zero-crossing, by acquiring data for 1 second. $|dS/d\mathrm{B}_{AC}|$ is determined from the slope of the curve near the zero crossing.

The AC sensitivity measurements using conventional readout, for XY8 (blue triangles) and DROID-60 (purple squares) are shown in Fig. S1(b). The total sensing duration is determined by the number of repetitions r of the sequence. The best sensitivity is achieved for DROID-60:6 and XY8:6 for total sensing durations of about 144 μs and 24 μs, respectively. With the XY8:6 sequence, we achieve very similar non-QLE AC sensitivity, 34(1) pT/$\sqrt{\mathrm{Hz}}$, as previously reported in our NV based nuclear magnetic resonance (NMR) measurements [5, 6], which were performed using largely the same apparatus as in the current work. We measure 47(1) pT/$\sqrt{\mathrm{Hz}}$ for the non-QLE AC sensitivity with correlation spectroscopy using XY8:6, slightly worse due to the deadtime introduced by T_{corr}. The DROID-60:6

sequence, with its longer sensing duration of 144 µs, outperforms the XY8:6 sequence, yielding a non-QLE sensitivity of 19.6(8) pT/$\sqrt{\text{Hz}}$, surpassing our previously reported NV-NMR AC sensitivities [5, 6].

The improved AC sensitivity achieved with DROID-60 is attributed to an extended NV electronic spin coherence time T_2 under DROID decoupling, as shown in Fig. S1(c) for both sequences. Under XY8 decoupling, the measured NV T_2 saturates at about 31 µs due to like-spin, NV-NV interactions (i.e., instantaneous diffusion), which are not decoupled by the XY8 sequence. Meanwhile, as previously demonstrated [3, 4], the DROID-60 sequence decouples such interactions, enabling increased T_2 with the application of additional decoupling cycles.

Our measured non-QLE AC sensitivity of 19.6(8) pT/$\sqrt{\text{Hz}}$, achieved using DROID-60:6, is comparable to the sensitivities reported from other state-of-the-art NV ensemble measurements, for example, 10.8 pT/$\sqrt{\text{Hz}}$ from Masuyama et al. [7] and 14.4 pT/$\sqrt{\text{Hz}}$ from Wolf et al. [8]. (The value from Ref. [8], 14.4 pT/$\sqrt{\text{Hz}}$, is the sensitivity when correctly calculated using the noise of only the readout window duration, rather than the total sequence duration. The total sequence duration includes long portions that do not contribute noise to the readout, and thus should not be included in calculating the sensitivity. This correction was previously reported in the literature, see note 20 in the Supplementary Information of [3]. Note: During the publication preparation stage, an Erratum to the Wolf et al. study was issued correcting their reported sensitivity to 9 pT/$\sqrt{\text{Hz}}$ [9].) Applying the largest QLE factor we measured with DROID-60:6, $\widetilde{\eta}_{\text{QLE}} = 5.7$, we calculate a QLE AC sensitivity of 3.4(1) pT/$\sqrt{\text{Hz}}$. For correlation spectroscopy with 2000 QLE readouts, we measure a sensitivity of 4.2(1) pT/$\sqrt{\text{Hz}}$, in agreement with $\widetilde{\eta}_{\text{QLE}} \approx 11$ from the signal-to-noise ratio (SNR) estimate in the main text.

We note that our measurements use a diamond interrogation volume of 2.3×10^3 µm^3, nearly 3 orders of magnitude smaller than the volumes used in Masuyama et al. and Wolf et al., which were 8.5×10^5 µm^3 and 1.4×10^6 µm^3, respectively. Thus, our system provides a volume normalized non-QLE AC sensitivity that is more than an order of magnitude better than in Masuyama et al. and Wolf et al. Our measurements use a smaller volume as the experimental system is primarily designed to measure micron-scale NMR samples, see Refs. [5, 6]. However, when employing the QLE protocol, a key constraint on the interrogation volume is homogeneity of the bias and control fields, as well as NV properties, as discussed in detail in the next section. Based on the performance of our current apparatus, we anticipate these homogeneity constraints can be readily satisfied for lateral dimensions of at least a few hundred micrometers without significant technical challenge, increasing the NV ensemble volume by about two orders of magnitude and thus improving the anticipated QLE AC sensitivity by about one order of magnitude.

IV. CONSIDERATIONS FOR IMPLEMENTING QUANTUM LOGIC READOUT IN NV ENSEMBLES

Applying the QLE protocol to an ensemble of pair-wise entangled qubits requires that the control fields and the qubits must be sufficiently identical across the ensemble. For our system of paired NV electronic spin and on-site ^{15}N nuclear spins, entanglement is facilitated by the hyperfine interaction, which is nominally identical for each NV in the ensemble. Our control fields are the bias magnetic, microwave (MW) drive, and radiofrequency (RF) drive fields. In order to apply uniform CNOT$_{e|n}$ gates to all the NVs in the ensemble, the NV hyperfine resonances must be clearly distinguished from each other (i.e., frequency resolved within their natural ODMR linewidth determined by $\Delta\nu \sim 1/\pi T_2^*$ in the absence of external inhomogeneities). Thus, variations in the hyperfine resonance frequencies across the NV ensemble, caused by inhomogeneity in the bias magnetic field and lattice strain, should be less than $\Delta\nu$ to ensure no additional linewidth broadening. The diamond used here has $T_2^* = 600$ ns, leading to a linewidth of $\Delta\nu \sim 0.5$ MHz, which is equivalent to a shift in bias magnetic field of ~ 200 mG. The magnetic field homogeneity for the same setup as used in the present experiment was previously characterized to be about 10 µT/mm [1], which is far better than that required for successful application of the QLE protocol. In addition, lattice strain in the type of CVD grown diamonds used in the present study was shown to induce <50 kHz variation in the NV ensemble hyperfine frequencies across areas $\sim 3 \times 3$ mm^2 [10], and thus, are also far from a limitation to successful use the QLE protocol.

The present experiments use a MW drive Rabi frequency (proportional to the MW field amplitude) of about 3.5 MHz. Relative to $\Delta\nu \sim 0.5$ MHz, this MW field amplitude can thus vary spatially across the NV ensemble by up to 15% without significantly contributing to pulse errors that degrade the fidelity of the CNOT$_{e|n}$ gates in the QLE protocol. For the 1 mm diameter loop used to apply the MW drive field, this homogeneity requirement is easily met across areas of up to 600×600 µm^2, as seen for the simulated MW and RF field strengths shown in Fig S2(a).

Homogeneity of the RF amplitude for the CNOT$_{n|e}$ gate is determined from a similar analysis. The frequency broadening by ~ 60 kHz of the RF pulse, from its finite duration ≈ 16.5 µs, is much greater than the nuclear spin linewidth ~ 50 Hz. Consequently, the estimated 4% spatial variation in the RF field strength across the NV layer, seen in Fig. S2(a), leads to a similar few percent imperfection of the CNOT$_{n|e}$ gate applied to the pair-wise entangled qubit ensemble.

Additionally, in order to achieve quantum logic sensitivity enhancement, the following must be satisfied: (i) optical readout duration less than the SWAP duration; (ii) SWAP duration less than the sensing duration. Short readout durations ($\sim$ few µs) are readily achievable with optical intensities $\sim 0.1 - 1.0$ mW/µm^2. Sufficiently short SWAP durations < 20 µs also readily achievable using commercially available RF amplifiers. As discussed in the main text, sensing durations are limited by the electronic spin coherence time T_2 of the NV ensemble, which can be extended using dynamical decoupling sequences. And finally, the nuclear T_1 can be extended by the application of large bias magnetic fields (as shown Fig. 2 in the main text). It should be emphasized, however, that the specific operational conditions and technical parameters used in this work are not required for quantum logic sensitivity enhancement. For example, referring to the main text Fig. 5(b), a nuclear spin $T_1 = 150$ µs (allowing ~ 50 readouts) can achieve a QLE sensitivity factor η_{QLE} of about $2\times$ to $6\times$, depending on the AC sensing sequence used.

Now we compare our NV ensemble QLE measurements to previous single NV work using a similar QLE protocol. In the demonstration by Jiang et al., the T_1 time of the ^{13}C spin memory qubit was only ~ 13 µs, with a readout duration of ~ 1 µs, limiting the observed SNR enhancement to about $2\times$[2]. In the work by Holzgrafe et al., the T_1 for the ^{14}N nuclear spin memory qubit was ~ 10 ms, at a bias magnetic field of ~ 2500 G, yielding a readout fidelity enhancement (equivalent to SNR enhancement) of about $13\times$ [11]. Typically the readout duration is dominated by the optical reinitialization time. However, Holzgrafe et al. included an additional error correction sequence in their protocol, leading their readout duration to be about 30 μs, which limited their observed readout enhancement. Lastly, the work by Lovchinsky et al. used ^{15}N as the nuclear spin memory qubit, with T_1 of about 1.5 ms (at bias magnetic field of ~ 2500 G) and a readout duration of about 1 µs, yielding a readout enhancement of $\sim 20\times$ [12]. As described in the main text and previously in this supplement, we used a dense NV ensemble over a length scale of ~ 15 µm, operated at a bias magnetic field of 3700 G and an incident laser power of 130 mW, and observed a quantum logic SNR enhancement of $\sim 33\times$ for all three AC sensing sequences studied, see Fig S2(b).

Quantum logic enhancements of measurement SNR and sensitivity are normalized to conventional NV optical readout under identical experimental conditions, and are thus independent of the optical characteristics of the apparatus, as long as the condition outlined above for the optical readout duration is satisfied. Technical features such as collection efficiency, objective numerical aperture, or detector choice will affect the measurement SNR and sensitivity achieved by the apparatus, for both conventional and quantum logic enhanced readout, but not the relative performance, i.e., the normalized enhancement.

It is expected that a similar QLE protocol should provide SNR and sensitivity enhancements for NV ensembles using the naturally abundant ^{14}N nuclear spin [11, 13]. The three NV hyperfine states associated with ^{14}N will reduce the fidelity of the SWAP operation, compared to the two NV hyperfine states for ^{15}N. In particular, NV ensemble SWAP fidelities of about 77% have been demonstrated for ^{14}N [14], compared to the estimated 93% fidelity in the present work using ^{15}N. Though this $\sim 15\%$ reduced fidelity using ^{14}N will limit the optimal number of optical readouts, significant quantum logic enhanced SNR and sensitivity should still be possible.

V. ^{15}N NUCLEAR SPIN T1

We characterize the ensemble ^{15}N nuclear spin lifetime T_1 under optical illumination in the experimental setup used throughout this work. After the nuclear spin SWAP at a bias magnetic field of 3700 G, the NV ensemble fluorescence contrast signal is measured as a function of variable optical pulse duration T_{op} at a fixed laser power incident to the diamond chip. The measurement protocol is shown in the inset of Fig. S3(a). The ^{15}N nuclear spins within each NV in the ensemble comprise a disordered system, where each spin experiences a different local environment. Thus, the use of a stretched exponential fit for extracting T_1 is more appropriate than a simple exponential, as shown in previous measurements of T_1 for ensembles of nuclear spins in diamond [16, 17]. Fitting the resulting NV fluorescence contrast decay data with a stretched exponential function, $a * \exp\left(-\left(\mathrm{T}_{op}/T_1\right)^c\right) + b$, yields the ensemble T_1 of the nuclear spins under optical illumination, where a, b, and c are fitting parameters. The procedure is repeated for various laser powers, with the resulting T_1 values as a function of laser power (black circles) shown in Fig. S3(a). The red curve in this figure is a power function model, $\alpha|x|^{-\beta} + \gamma$, with fit parameters $\alpha = 4.003 \times 10^4$, $\beta = 0.5154$, and $\gamma = 111$. The stretch exponent values from the fits are shown for both laser power and magnetic field dependent T_1 measurements in Figs. S3 (b) and (c), respectively. Finally, decay data and fits for all the T_1 laser power and magnetic field dependent measurements are shown in Figs. S4 and S5, respectively.

While Fig. S3 suggests it would be ideal to work at lower laser power (for a fixed illumination area), as the ^{15}N nuclear spin T_1 is longer at lower laser powers, one must also consider the need for longer optical polarization pulses at lower laser powers in order to repolarize the NV electronic spin. For QLE sensing, the performance of the technique (including AC magnetic field sensitivity) is optimized by maximizing the number of readout pulses. This can be

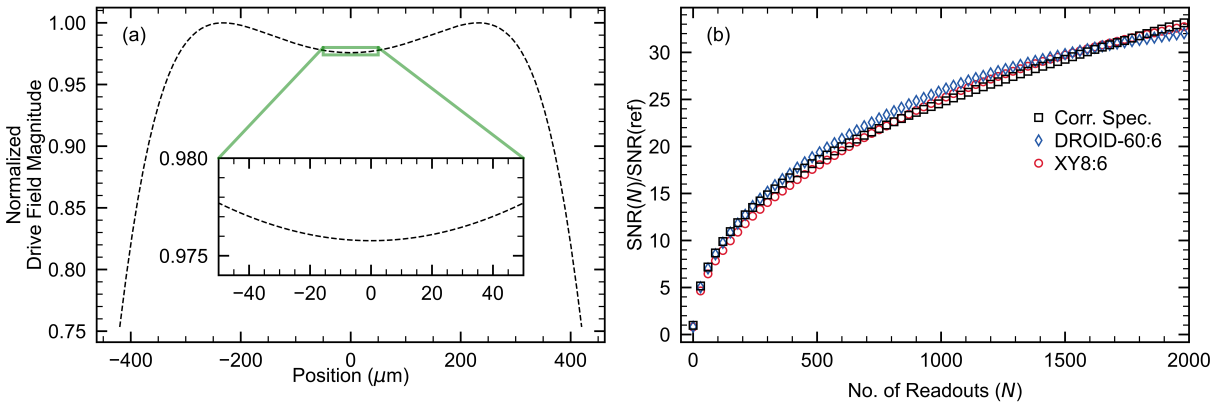


FIG. S2. **Drive field homogeneity from a 1 mm loop and quantum logic enhancement of Signal-to-Noise Ratio (SNR).** (a) Calculated transverse spatial profile of the magnetic field normal component generated by a 1 mm diameter loop at an offset distance of 0.5 mm from the NV ensemble, as shown by the gray, single loop antenna in Fig. 1 of the main text. Position 0 µm corresponds to the point in space 0.5 mm below the loop center, with the plotted position corresponding to moving transversely outward from this 0 µm position. The inset shows the field profile in a ±50 µm region around the loop center, yielding an estimated transverse homogeneity ≈ 0.05 % for the MW and RF drive field magnitudes across the ∼ 15 µm wide NV ensemble probed in the present experiment. Along the ∼ 13 µm depth of the NV layer, the estimated MW and RF drive field homogeneity ≈ 4%, given a standoff distance of about 0.5 mm between the loop and the NV layer. To show variation in field strength, the field is normalized to the largest value within this spatial range. The field pattern was simulated with Magpylib [15]. (b) Improvement in SNR of the measured 1 MHz test signal as a function of the number of quantum logic readout (QLR) cycles, N, compared to the reference SNR of a single readout sequence without the QLE protocol. Similar results are found for the three AC magnetic field sensing sequences used in the present study.

achieved by reducing the duration of each readout/repolarization pulse (i.e., increasing the laser power) and also increasing the ^{15}N T_1 (i.e., decreasing the laser power). To balance these two factors, we choose to work at a laser power of 130 mW where ∼ 75% of the NV electronic spins are repolarized within 2.7 µs.

[1] D. R. Glenn, D. B. Bucher, J. Lee, M. D. Lukin, H. Park, and R. L. Walsworth, High-resolution magnetic resonance spectroscopy using a solid-state spin sensor, Nature **555**, 351 (2018).

[2] L. Jiang, J. S. Hodges, J. R. Maze, P. Maurer, J. M. Taylor, D. G. Cory, P. R. Hemmer, R. L. Walsworth, A. Yacoby, A. S. Zibrov, and M. D. Lukin, Repetitive readout of a single electronic spin via quantum logic with nuclear spin ancillae, Science **326**, 267 (2009).

[3] H. Zhou, J. Choi, S. Choi, R. Landig, A. M. Douglas, J. Isoya, F. Jelezko, S. Onoda, H. Sumiya, P. Cappellaro, H. S. Knowles, H. Park, and M. D. Lukin, Quantum metrology with strongly interacting spin systems, Phys. Rev. X **10**, 031003 (2020).

[4] J. Choi, H. Zhou, H. S. Knowles, R. Landig, S. Choi, and M. D. Lukin, Robust dynamic hamiltonian engineering of many-body spin systems, Phys. Rev. X **10**, 031002 (2020).

[5] D. B. Bucher, D. R. Glenn, H. Park, M. D. Lukin, and R. L. Walsworth, Hyperpolarization-enhanced nmr spectroscopy with femtomole sensitivity using quantum defects in diamond, Phys. Rev. X **10**, 021053 (2020).

[6] N. Arunkumar, D. B. Bucher, M. J. Turner, P. TomHon, D. Glenn, S. Lehmkuhl, M. D. Lukin, H. Park, M. S. Rosen, T. Theis, and R. L. Walsworth, Micron-scale nv-nmr spectroscopy with signal amplification by reversible exchange, PRX Quantum **2**, 010305 (2021).

[7] Y. Masuyama, K. Mizuno, H. Ozawa, H. Ishiwata, Y. Hatano, T. Ohshima, T. Iwasaki, and M. Hatano, Extending coherence time of macro-scale diamond magnetometer by dynamical decoupling with coplanar waveguide resonator, Review of Scientific Instruments **89**, 125007 (2018).

[8] T. Wolf, P. Neumann, K. Nakamura, H. Sumiya, T. Ohshima, J. Isoya, and J. Wrachtrup, Subpicotesla diamond magnetometry, Phys. Rev. X **5**, 041001 (2015).

[9] T. Wolf, P. Neumann, K. Nakamura, H. Sumiya, T. Ohshima, J. Isoya, and J. Wrachtrup, Erratum: Subpicotesla diamond magnetometry [phys. rev. x 5, 041001 (2015)], Phys. Rev. X **13**, 029903 (2023).

[10] A. M. Edmonds, C. A. Hart, M. J. Turner, P.-O. Colard, J. M. Schloss, K. S. Olsson, R. Trubko, M. L. Markham, A. Rathmill, B. Horne-Smith, W. Lew, A. Manickam, S. Bruce, P. G. Kaup, J. C. Russo, M. J. DiMario, J. T. South, J. T. Hansen, D. J. Twitchen, and R. L. Walsworth, Characterisation of CVD diamond with high concentrations of nitrogen for

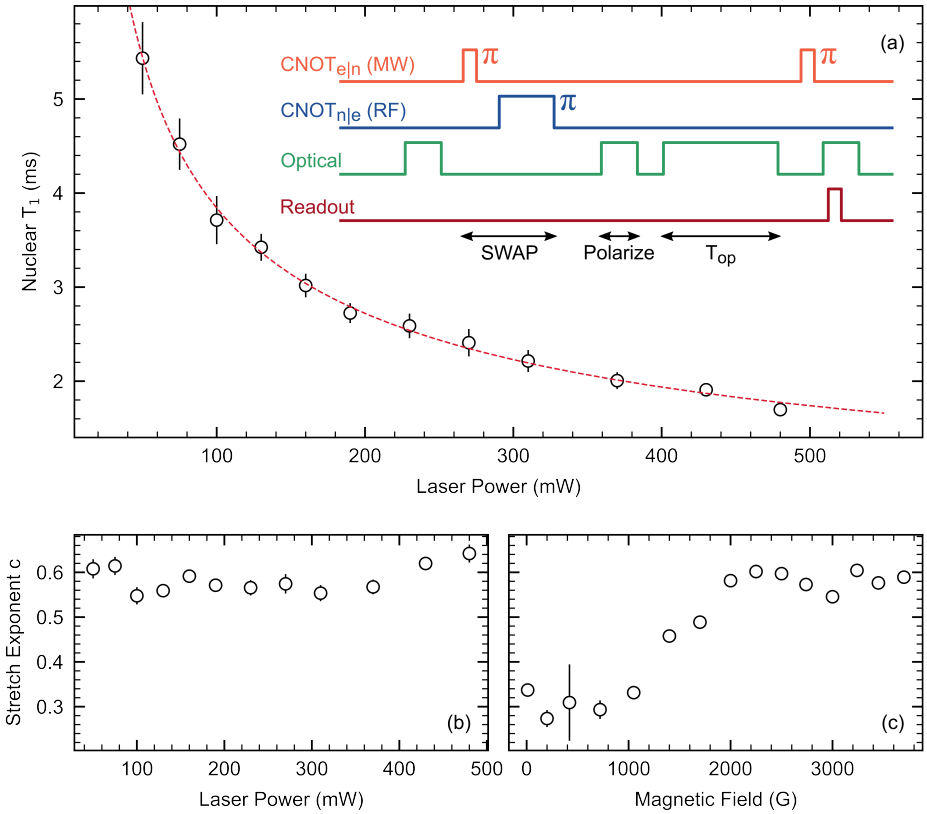


FIG. S3. **Laser power vs ensemble ^{15}N nuclear spin T_1 and and stretch exponent values from fits**. (a) ^{15}N nuclear spin T_1 at bias magnetic field of 3700 G, as a function of laser power, extracted from stretched exponential fits. Inset shows the pulse sequence used in these measurements. (b) and (c) show the stretch exponent values, extracted from fits, for the laser power and magnetic field dependent measurements, respectively. A fixed laser illumination spot of $\sim$ 15 µm in diameter was used.

magnetic-field sensing applications, Materials for Quantum Technology **1**, 025001 (2021).
[11] J. Holzgrafe, J. Beitner, D. Kara, H. S. Knowles, and M. Atatüre, Error corrected spin-state readout in a nanodiamond, npj Quantum Information **5**, 10.1038/s41534-019-0126-2 (2019).
[12] I. Lovchinsky, A. O. Sushkov, E. Urbach, N. P. de Leon, S. Choi, K. De Greve, R. Evans, R. Gertner, E. Bersin, C. Müller, L. McGuinness, F. Jelezko, R. L. Walsworth, H. Park, and M. D. Lukin, Nuclear magnetic resonance detection and spectroscopy of single proteins using quantum logic, Science **351**, 836 (2016).
[13] P. Neumann, J. Beck, M. Steiner, F. Rempp, H. Fedder, P. R. Hemmer, J. Wrachtrup, and F. Jelezko, Single-shot readout of a single nuclear spin, Science **329**, 542 (2010).
[14] V. V. Soshenko, S. V. Bolshedvorskii, O. Rubinas, V. N. Sorokin, A. N. Smolyaninov, V. V. Vorobyov, and A. V. Akimov, Nuclear spin gyroscope based on the nitrogen vacancy center in diamond, Phys. Rev. Lett. **126**, 197702 (2021).
[15] M. Ortner and L. G. Coliado Bandeira, Magpylib: A free python package for magnetic field computation, SoftwareX 10.1016/j.softx.2020.100466 (2020).
[16] A. Ajoy, B. Safvati, R. Nazaryan, J. Oon, B. Han, P. Raghavan, R. Nirodi, A. Aguilar, K. Liu, X. Cai, et al., Hyperpolarized relaxometry based nuclear t1 noise spectroscopy in diamond, Nature communications **10**, 1 (2019).
[17] R. Wunderlich, R. Staacke, W. Knolle, B. Abel, J. Haase, and J. Meijer, Robust nuclear hyperpolarization driven by strongly coupled nitrogen vacancy centers, Journal of Applied Physics **130**, 104301 (2021).

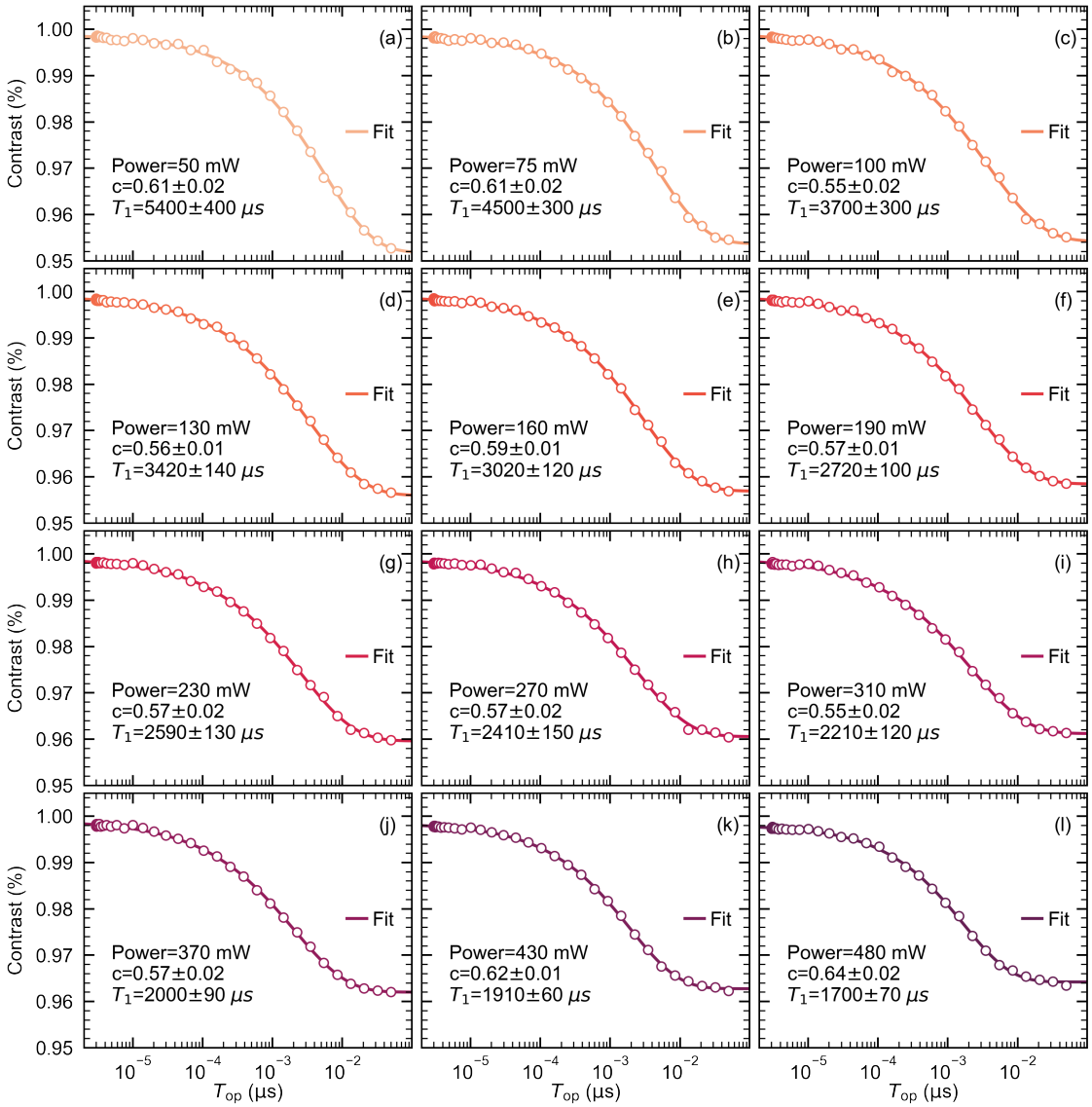


FIG. S4. **^{15}N nuclear spin decays for varying laser power fit to stretched exponential functions.** The ^{15}N nuclear spin decays are determined from the measurements of the NV ensemble fluorescence contrast signal as a function of optical pulse duration T_{op}, using the sequence shown in the inset of Fig. S3 (a). A fixed laser illumination spot of $\sim$ 15 μm in diameter and a magnetic field of 3700 G were used for all measurements shown here.

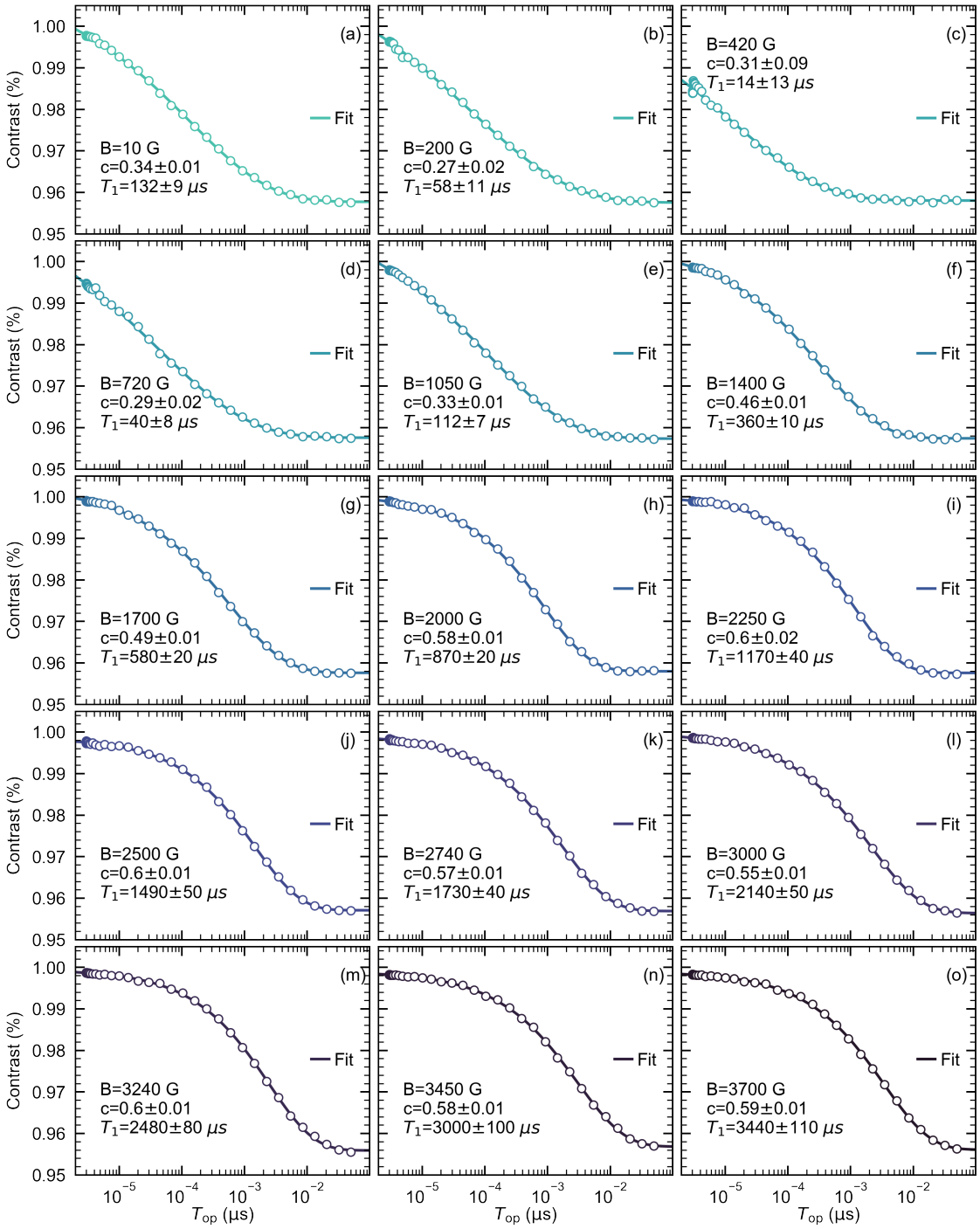


FIG. S5. **^{15}N nuclear spin decays for varying magnetic field fit to stretched exponential functions**. The ^{15}N nuclear spin decays are determined from the measurements of the NV ensemble fluorescence contrast signal as a function of optical pulse duration T_{op}, using the sequence shown in the inset of Fig. S3 (a). A fixed laser illumination spot of $\sim$ 15 μm in diameter and a laser power of 130 mW were used for all measurements shown here.